Int. J. Electrochem. Sci., 16 **(2021)** Article ID: 210335, doi: 10.20964/2021.03.49

International Journal of
ELECTROCHEMICAL
SCIENCE
www.electrochemsci.org

1-Phenyl-1H-tetrazol as Corrosion Inhibitor for Pipeline Steel in Sulfuric Acid Solution

Shiying Tao[1,2,3,*]

[1] Faculty of Science and Engineering, The University of Nottingham Ningbo China, Ningbo 315100, PR China
[2] Ningbo Nottingham New Materials Institute Ltd., Ningbo 315040, PR China
[3] School of Materials and Chemical Engineering, Ningbo University of Technology, Ningbo 315211, PR China
[*]E-mail: sytao_nbu@163.com, Carey.Tao@nottingham.edu.cn

Received: 15 November 2020 / *Accepted:* 6 January 2021 / *Published:* 31 January 2021

1-Phenyl-1H-tetrazol (PHT) has been studied as an efficient corrosion inhibitor for X65 steel in sulfuric acid corrosion environment. Atomic force microscope test results show that PHT can effectively inhibit the corrosion of X65 steel in 0.5 M sulfuric acid solution. Quantum chemical calculations and molecular dynamics simulations show that PHT has a small energy gap value and a large dipole moment value, which is an excellent corrosion inhibitor. In addition, the adsorption of PHT on the Fe(110) surface adopts parallel adsorption and a large binding energy value, which shows that PHT can effectively inhibit the corrosion of X65 steel. Potentiodynamic polarization test results show that as the PHT concentration increases, the value of the corrosion current density decreases significantly. When the PHT concentration is 1 mM, the corrosion inhibition efficiency can reach 92.1%. In addition, the adsorption of PHT on the surface of X65 steel conforms to Langmuir adsorption, and the adsorption process is spontaneous.

Keywords: Corrosion inhibitor, X65 steel, Molecular dynamics simulation, Quantum chemical calculation, AFM

1. INTRODUCTION

The corrosion of metals has always restricted the progress and development of human society. Metal corrosion will bring a lot of economic losses and even serious safety accidents every year. With the continuous progress and development of human society, scientists have explored many ways to combat metal corrosion [1]. Common corrosion protection methods include coating, sacrificial anode protection, and the development of new alloys. The use of corrosion inhibitors to protect metals has been loved by corrosion scientists. This is because corrosion inhibitors have unique advantages in many aspects. For example, corrosion inhibitors are extremely convenient to use, and can still play a good

protective role in many severe corrosive environments. In addition, the cost of corrosion inhibitors is also much lower for other corrosion protection methods. Therefore, corrosion inhibitors have been widely used. The corrosion inhibitor contains nitrogen (N), sulfur (S), oxygen (O), phosphorus (P) and other heteroatoms and a large number of electron donating groups to give lone electron pairs [2-6]. Thus showing excellent corrosion inhibition performance.

In recent years, Gao et al. [7] studies have studied the corrosion inhibition performance of papain on copper in sulfuric acid solution. When the concentration of papain is 5 mM, its corrosion inhibition efficiency can reach 98.5% at 298 K. Zhang et al. [8] studied the corrosion inhibition performance of 2-(3H-Imidazol-4-yl)-ethylamine as a corrosion inhibitor on Q235 steel in hydrochloric acid solution. When the concentration of HIE reaches 5 Mm, its corrosion inhibition efficiency can reach 93.1% at a temperature of 298 K. Li et al. [9] studied the corrosion inhibition performance of 5-(4-methoxyphenyl)-3h-1, 2-dithiole-3-thione as a corrosion inhibitor on steel in acidic solutions. When the concentration of MDT is 80 ppm, its corrosion inhibition efficiency is 80.3% at 298 K. In addition, the corrosion inhibition efficiency of MDT increases with increasing temperature. Chen et al. [10] studied the corrosion inhibition performance of Coconut Leaf Extract on X65 steel in hydrochloric acid corrosion media. Electrochemical experiment results show that when the concentration of CLE is 400 ppm, its corrosion inhibition efficiency can reach 94.1%.

In this work, i studied the corrosion inhibition performance of 1-Phenyl-1H-tetrazol (PHT) on X65 steel in 0.5 M sulfuric acid solution. I used a variety of experimental methods for research. These experiments include 3D morphology, quantum chemistry calculations and molecular dynamics simulations, as well as open circuit potential, electrochemical impedance spectroscopy, Potentiodynamic polarization test and other methods. The corrosion inhibition performance of 1-Phenyl-1H-tetrazol on X65 steel was studied from multiple angles.

2. EXPERIMENTAL

2.1 Test materials

The test in this paper is that X65 steel belongs to pipeline steel for natural transportation. Its composition is Mn 1.6%, Si 0.18%, Cr 0.17%, C 0.05%, Nb 0.04%, Al 0.03%, and the remainder is Fe. The chemical structure of 1-Phenyl-1H-tetrazol is shown in Figure 1. Its purity is greater than 99%, and it is used without further treatment.

PHT is formulated into 0.1, 0.2, 0.5, 1 mM test solution for use. X65 steel is cut into cylinders with a diameter of 1 cm for making working electrodes. In the process of electrode packaging, the cut sample is polished on 180-mesh sandpaper. The polished X65 steel is sealed with epoxy resin, leaving one side exposed to the corrosive solution. X65 steel was cut into $0.8 \times 0.8 \times 0.1$ cm samples for atomic force microscope testing. X65 steel is polished with 180 to 3000 mesh sand paper in turn. After polishing, the X65 steel was soaked in a PHT solution containing and lacking 1 mM for 2 hours, and then the surface morphology was tested.

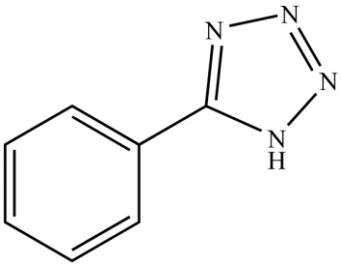

Figure 1. The molecular structure of 1-Phenyl-1H-tetrazol.

2.2 Electrochemical test

The electrochemical experiment of PHT was tested using Chenhua Chi604D electrochemical workstation in a three-electrode system. Among them, X65 steel was polished to 1200 mesh in turn before the test, it is the working electrode. The saturated calomel electrode is the reference electrode, and the platinum plate is the counter electrode. Prepare a new solution before each electrochemical test. The open circuit test takes 1200 seconds to ensure that the X65 steel surface reaches a stable state. The initial potential of the electrochemical impedance spectroscopy test is a stable open circuit voltage. The frequency range of the test is from 100000 Hz at high frequency to 0.01 Hz at low frequency. The polarization range of the Potentiodynamic polarization test is from E_{OCP}−250 mV to E_{OCP}−250 mV, and the polarization rate is 2 mV/s.

3.3 Details of quantum chemistry calculations and molecular dynamics simulation calculations

The dipole moment, frontier molecular orbital, and electrostatic potential diagram of PHT are calculated using Material Studio software (MS) software. Adopt Dmol3 as the calculation module, structure optimization as the calculation task. DNP is set as the basis set. The adsorption of PHT on the Fe(110) surface uses the Forcite module. Fill a PHT molecule and 350 water molecules into the 3D model. Optimize the structure of the filled system and perform molecular dynamics simulation after optimization. The simulation time is 300 ps to ensure the stable adsorption of PHT on the Fe(110) surface.

3. RESULTS AND DISCUSSION

3.1 3D topography analysis

Figure 2 shows the 3D surface morphology of X65 steel immersed in the 0.5 M sulfuric acid environment with and without 1 mM PHT at a temperature of 298 K and a immersion time of 2 hours. As shown in Figure 2(a), when X65 steel is immersed in a corrosion solution containing PHT, its surface is still very flat, just like the one just after polishing. The surface roughness of X65 steel is 3.31 nanometers. As shown in Figure 2(b), when X65 steel is immersed in 0.5 M sulfuric acid solution, the

entire surface of X65 steel appears corroded like a hilly area. The entire X65 steel was severely corroded by sulfuric acid, and the surface roughness of the entire X65 steel was 24.2 nanometers. The comparison can prove that PHT can effectively inhibit the corrosion of X65 steel.

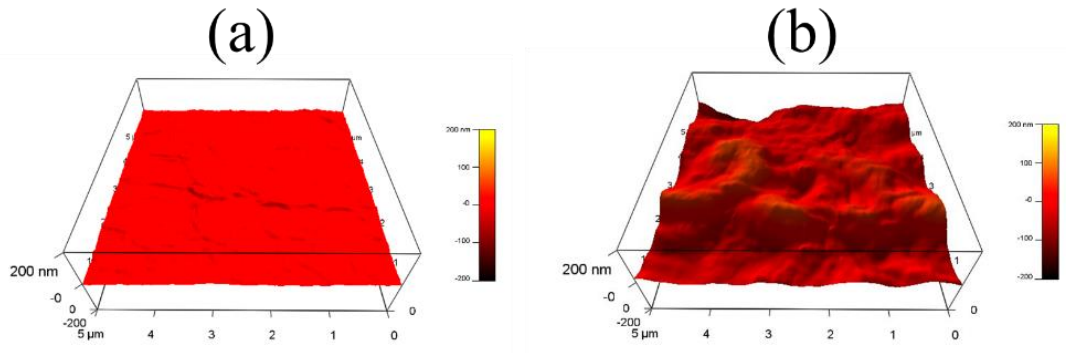

Figure 2. The surface morphology of X65 steel at 298 K after being immersed in 0.5 M sulfuric acid solution for 2 h at 298 K (a) containing and (b) lacking 1 mM PHT.

3.2 Quantum Chemistry Computational Research

Figure 3 presents the optimized molecular configuration, electrostatic potential diagram, and frontline molecular orbital diagram after PHT optimization. As shown in Figure 3, after PHT optimization, the benzene ring and the nitrogen-containing five-membered ring are on the same plane, which is conducive to the parallel adsorption of PHT molecules on the X65 steel surface to obtain a large coverage. The electrostatic potential diagram consists of the blue area of the benzene ring and the dark red area of the nitrogen-containing five-membered ring. The blue area has electrophilic properties, and the dark red area has nucleophilic properties [11]. Therefore, it can be shown that the nitrogen-containing five-membered ring is easier to donate electrons and form coordination bonds with X65 steel. In addition, it can be found that the electrons of the HOMO orbital and LUMO orbital of PHT are distributed throughout the molecule. As all know, the HOMO orbital represents the electron donating ability of PHT molecules, and the LUMO orbital corresponds to the electron receiving ability of PHT molecules [12, 13]. I calculated the energy gap value of the PHT molecule to be 4.02 eV. This is a small energy gap value, indicating that PHT can exhibit excellent corrosion inhibition performance [14]. The dipole moment of PHT is 6.19 D. The large dipole moment value indicates that PHT can effectively change the electric double layer capacitance on the surface of X65 steel when adsorbed on the surface of X65 steel, thus exhibiting excellent corrosion inhibition performance.

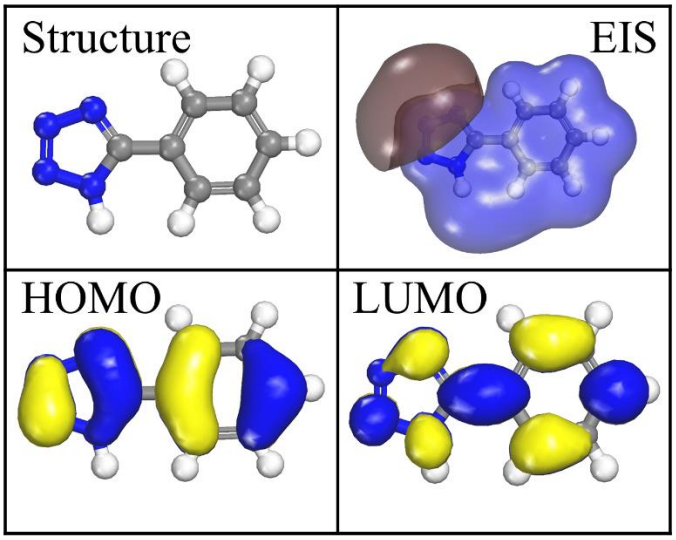

Figure 3. PHT optimized molecular structure, frontline molecular orbital and electrostatic potential diagram.

3.3 Molecular dynamics simulation research

Figure 4 shows the top view and side view of PHT after adsorption on the Fe(110) surface. As shown in Figure 4, we can find that PHT adopts a parallel adsorption configuration after adsorption on the Fe(110) surface to obtain the maximum coverage, thereby effectively inhibiting the corrosion of X65 steel in sulfuric acid solution. This is consistent with the predicted result of quantum chemistry. In addition, in order to further analyze the binding energy of PHT and X65 steel surface, the following formulas to calculate binding energy [15, 16]:

$$E_{interact} = E_{tot} - (E_{subs} + E_{inh}) \quad (1)$$

$$E_{binding} = -E_{interact} \quad (2)$$

Among them, the value of E_{tot} is –2039.4 kcal/mol, the value of E_{sub} is –2016.2 kcal/mol, and the value of E_{inh} is –75.2 kcal/mol. Substituting formulas 1 and 2 can find that the binding energy value is 98.4 kcal/mol. A large binding energy value indicates that the surface of PHT and X65 steel has a strong adsorption effect.

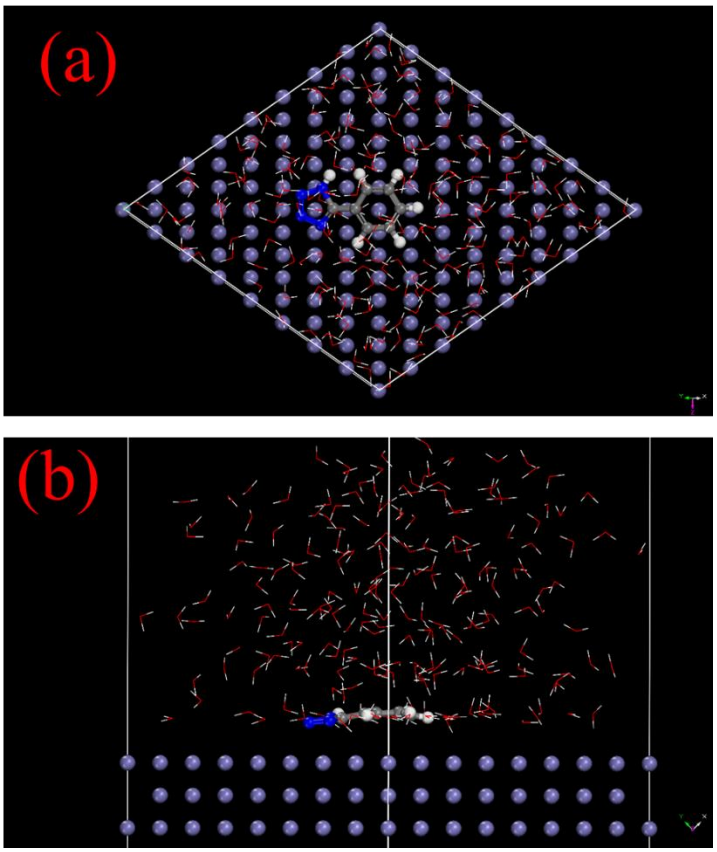

Figure 4. The stable configuration of PHT adsorption on Fe(110) surface; (a) Top view, (b) Side view.

3.4 Electrochemical test

Figure 5 presents the electrochemical impedance spectra of X65 steel immersed in 0.5 M sulfuric acid solution containing different concentrations of PHT. As shown in Figure 5, as the concentration of PHT increases, the diameter of the capacitive reactance increases significantly, which indicates that PHT can inhibit the charge transfer resistance after adsorption on the surface of X65 steel. In addition, it can be found that when the concentration of PHT is 0.5 mM, the inductive arc in the low frequency region obviously disappears, which indicates that the adsorption of PHT can effectively inhibit the diffusion of iron ions into the sulfuric acid solution, thereby exhibiting good corrosion inhibition performance. Figure 6 shows the impedance modulus diagram and phase angle diagram of X65 steel immersed in 0.5 M sulfuric acid solution containing different concentrations of PHT. It can be found that with the increase of PHT concentration, the impedance modulus value and the phase angle value become higher and wider, which proves that PHT is an effective corrosion inhibitor.

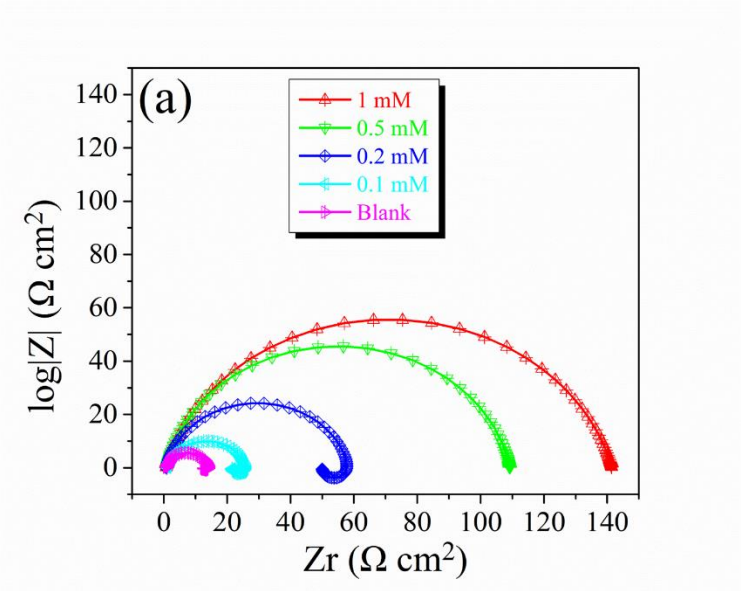

Figure 5. Electrochemical impedance spectra of X65 steel immersed in 0.5 M sulfuric acid solution at 298 K with different concentrations of PHT.

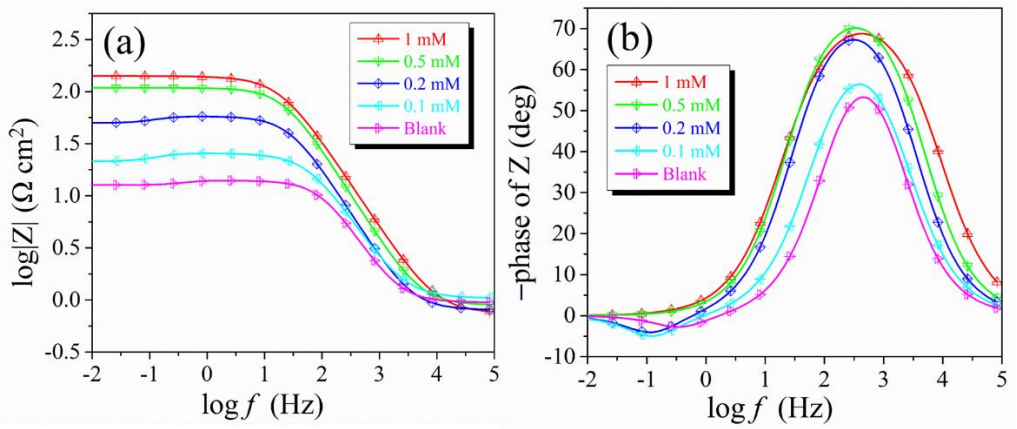

Figure 6. (a) Impedance modulus diagram and (b) phase angle diagram of X65 steel immersed in 0.5 M sulfuric acid solution at 298 K containing different concentrations of PHT.

In order to quantitatively analyze the EIS data, we used the equivalent circuit diagram in Figure 7 to fit the EIS data. The fitted data are listed in Table 1. The corrosion inhibition efficiency in Table 1 can be calculated by the following formula [17-23]:

$$\eta(\%) = \frac{R_{ct} - R_{ct,0}}{R_{ct}} \times 100 \qquad (3)$$

When the concentration of PHT is 0.1, 0.2, 0.5, 1mM, the corrosion inhibition efficiency of PHT is 46.9%, 77.3%, 87.9% and 90.7%, respectively. The charge transfer resistance increased sharply from the blank 13.1 Ω cm^2 to 140.7 Ω cm^2. In addition, the solution resistance in the blank solution is 0.98 Ω cm^2. When PHT is added, the solution resistance shows a downward trend, which indicates that PHT has a certain conductivity.

The last thing worth mentioning is the electric double layer capacitance. The value of the electric double layer capacitance in the blank solution is 208.9 μF cm^{-2}. After adding 0.1, 0.2, 0.5, 1 mM PHT in the sulfuric acid solution, the electric double layer capacitance The values of are 167.3, 123.1, 91.3, 80.7 μF cm^{-2}, respectively. Therefore, the electric double layer capacitance shows a downward trend. According to the definition of the electric double layer capacitance, it can be found that the more water on the surface of the X65 steel replaced by PHT, the more obvious the decrease in the value of the electric double layer capacitance and the better the corrosion inhibition performance.

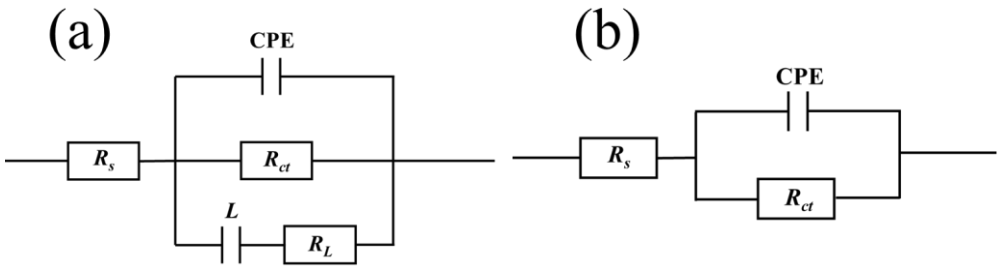

Figure 7. Equivalent circuit diagram for fitting electrochemical impedance spectroscopy.

Table 1. EIS data fitted with equivalent circuit diagram for pipeline steel immersed in 0.5 M sulfuric acid solution containing different concentrations of PHT.

C (mM)	R_s (Ω cm^2)	$Y_0\times10^{-6}$ (S s^n cm^{-2})	n	C_{dl} (μF cm^{-2})	R_{ct} (Ω cm^2)	L (Ω cm^2)	R_L (Ω cm^2)	η (%)
Blank	0.98	228.4	0.89	208.9	13.1	48.1	107.3	/
0.1	0.84	190.1	0.86	167.3	24.7	162.2	118.1	46.9
0.2	0.80	123.2	0.89	123.1	57.6	47.6	337.2	77.3
0.5	0.89	112.9	0.90	91.3	108.4	/	/	87.9
1.0	0.74	98.6	0.85	80.7	140.7	/	/	90.7

Figure 8 shows the open circuit potential diagram of X65 steel immersed in sulfuric acid solution. It can be clearly found that the open circuit potential is obviously stable after 1200 seconds of testing, which means that the surface of X65 steel has reached a stable condition. It is also worth mentioning that the change trend of the open circuit voltage after adding HPT is not obvious compared to the blank solution. This shows that HPT did not change the reaction mechanism of the X65 steel cathode and anode. Figure 9 shows that the Potentiodynamic polarization diagram of X65 steel immersed in 0.5 M sulfuric acid solution contains different concentrations of HPT. It can be clearly found that the corrosion current density decreases significantly as the HPT concentration increases. The Tafel extrapolation method to list the obtained polarization curve parameters in Table 2. The corrosion inhibition efficiency can be obtained by the following formula [24-32]:

$$\eta(\%) = \frac{i_{corr,0} - i_{corr}}{i_{corr,0}} \times 100 \qquad (2)$$

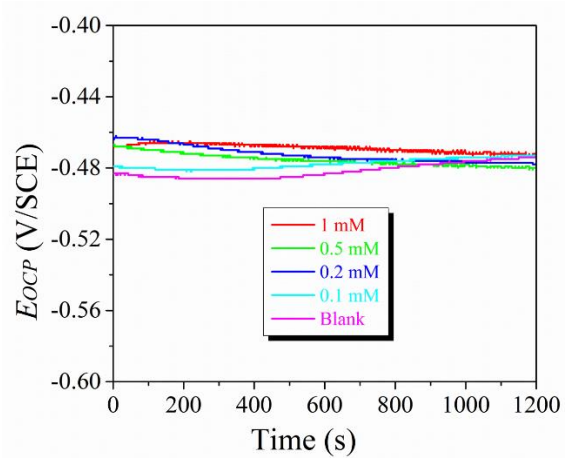

Figure 8. The open circuit potential diagram of X65 steel immersed in 0.5 m sulfuric acid solution at 298 K contains different concentrations of HPT.

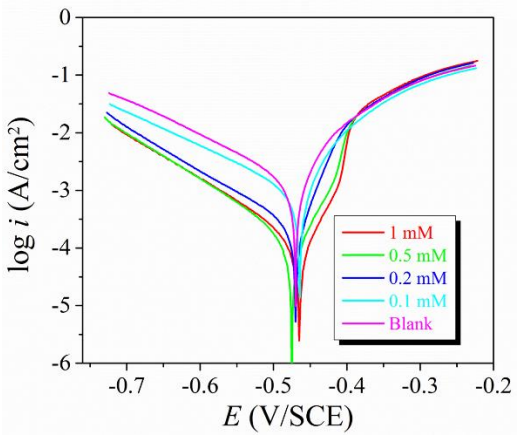

Figure 9. The Potentiodynamic polarization curve of X65 steel immersed in 0.5 M sulfuric acid solution at 298 K contains different concentrations of HPT.

Table 2. Potentiodynamic polarization curve parameters obtained by Tafel extrapolation way for pipeline steel immersed in 0.5 M sulfuric acid solution containing different concentrations of PHT.

C (mM)	E_{corr}(V/SCE)	i_{corr}(mA cm^{-2})	β_c(mV dec^{-1})	β_a(mV dec^{-1})	η (%)
Blank	–0.470	2.16	–154	115	/
0.1	–0.464	1.10	–160	105	49.1
0.2	–0.470	0.47	–141	96	78.2
0.5	–0.475	0.23	–120	79	89.3
1.0	–0.465	0.17	–124	67	92.1

As shown in Table 2, the corrosion current density in the blank solution is 2.16 mA cm^{-2}. When the concentration of HPT is 0.1, 0.2, 0.5, and 1 mM, the corrosion current density at this time is 1.1, 0.47, 0.23, 0.17 mA cm^{-2}.

The corrosion inhibition efficiencies at this time are 49.1%, 78.2%, 89.3%, and 92.1% respectively. It is also worth mentioning that the cathodic branches show a parallel trend, which indicates that the adsorption of HPT on the surface of X65 steel does not change the precipitation of hydrogen ions at the cathode. The change trend of corrosion potential is less than 85 mV, indicating that HPT is a mixed corrosion inhibitor [33, 34].

3.5 Research on isothermal adsorption model

The adsorption mechanism of PHT on the surface of X65 steel has been studied using a variety of adsorption isotherm models. The adsorption of PHT on the surface of X65 steel conforms to Langmuir isotherm adsorption. The formula of Langmuir isotherm adsorption is as follow [35-39]:

$$\frac{C}{\theta} = \frac{1}{K_{ads}} + C \qquad (3)$$

The linear regression coefficient after fitting is 0.9954. Therefore, it can be shown that PHT conforms to Langmuir single-layer adsorption on the surface of X65 steel. The adsorption equilibrium constant is 13157.9 L/mol. The large adsorption constant indicates that the surface of PHT and X65 steel has a strong binding force. In order to study the adsorption type of PHT on the surface of X65 steel, we calculated the adsorption Gibbs free energy, its expression is as follow [40, 41]:

$$K_{ads} = \frac{1}{1000}\exp(-\frac{\Delta G^0_{ads}}{RT}) \qquad (4)$$

The calculated Gibbs free energy value is −33.4 kJ/mol, When the absolute value of Gibbs free energy is less than 20 kJ/mol, it is physical adsorption [42]. The adsorption Gibbs free of HPT on the surface of X65 steel is between 20 and 40 kJ/mol, so it belongs to both physical and chemical adsorption.

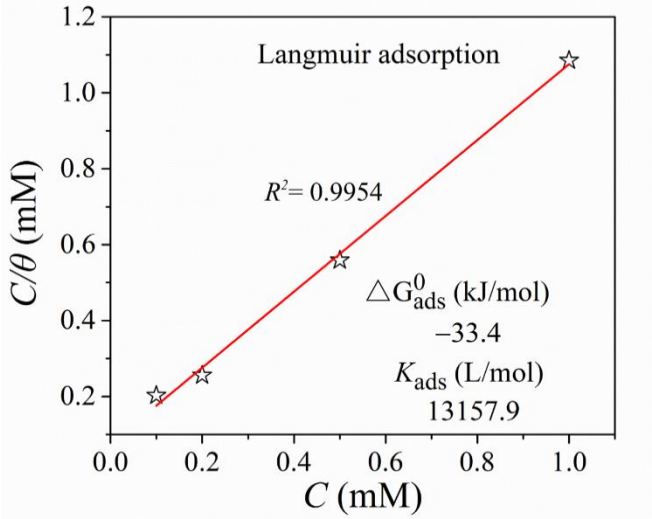

Figure 10. Langmuir adsorption isotherm diagram.

4. CONCLUSION

The surface tested by atomic force microscope indicted HPT can effectively inhibit the corrosion of X65 steel in 0.5 M sulfuric acid solution. Quantum chemical calculations show that HPT has a large dipole moment and a small energy gap value, and can exhibit excellent corrosion inhibition. Electrochemical test results show that HPT is a mixed corrosion inhibitor, which can simultaneously inhibit the reaction of X65 steel cathode and anode. The adsorption isotherm model research shows that the adsorption of HPT on the surface of X65 steel is a combination of physical and chemical adsorption, and is consistent with Langmuir adsorption.

ACKNOWLEDGMENTS
This work was supported financially by Department of Education of Zhejiang Province(Y201941937).

References

1. W. Sun, Y. Liu, T. Li, S. Cui, S. Chen, Q. Yu, and D. Wang, *J. Colloid Interf. Sci*., 554 (2019) 488.
2. B. Tan, J. He, S. Zhang, C. Xu, S. Chen, H. Liu, and W. Li, *J. Colloid Interf. Sci*., 585 (2021) 287.
3. Ž.Z. Tasić, M.B. Petrović Mihajlović, M.B. Radovanović, A.T. Simonović, and M.M. Antonijević, *J. Mol. Struct*., 1159 (2018) 46.
4. Ž.Z. Tasić, M.B. Petrović Mihajlović, M.B. Radovanović, and M.M. Antonijević, *J. Mol. Liq*., 265 (2018) 687.
5. M.B. Petrović Mihajlović, and M. M. Antonijevic, *Int. J. Electrochem. Sci.*, 3 (2008) 1
6. W. Zhang, H. Li, M. Wang, L. Wang, Q. Pan, X. Ji, Y. Qin, and Y. Wu, *J. Mol. Liq*., 293 (2019) 111478.
7. L. Gao, S. Peng, X. Huang, and Z. Gong, *Appl. Surf. Sci*., 511 (2020) 145446.
8. J. Zhang, *Int. J. Electrochem. Sci*., 15 (2020) 1437.
9. Q. Li, *Int. J. Electrochem. Sci*., 15 (2020) 12534.
10. S. Chen, B. Zhu, and X. Liang, *Int. J. Electrochem. Sci*., 15 (2020) 1
11. B. Tan, S. Zhang, Y. Qiang, W. Li, H. Li, L. Feng, L. Guo, C. Xu, S. Chen, and G. Zhang, *J. Mol. Liq*., 298 (2020) 111975.
12. B. Tan, B. Xiang, S. Zhang, Y. Qiang, L. Xu, S. Chen, and J. He, *J. Colloid Interf. Sci*., 582 (2020) 918.
13. Z. Xiao, Z. Zhou, L. Song, D. Wu, C. Zeng, and Z. Cao, *Int. J. Electrochem. Sci*., 14 (2019) 4705.
14. B. Tan, S. Zhang, Y. Qiang, W. Li, H. Liu, C. Xu, and S. Chen, *J. Mol. Liq*., 286 (2019) 110891.
15. B. Tan, S. Zhang, H. Liu, Y. Qiang, W. Li, L. Guo, and S. Chen, *J. Taiwan Inst. Chem. E*., 102 (2019) 424.
16. K.R. Ansari, D.S. Chauhan, M.A. Quraishi, and T.A. Saleh, *J. Colloid Interf.Sci.*, 564 (2020) 124.
17. B. Tan, S. Zhang, H. Liu, Y. Guo, Y. Qiang, W. Li, L. Guo, C. Xu, and S. Chen, *J. Colloid Interf. Sci.*, 538 (2019) 519.
18. X. Wang, H. Jiang, D. Zhang, L. Hou, and W. Zhou, *Int. J. Electrochem. Sci*., 14 (2019) 1178.
19. N. V. Likhanova, P. Arellanes-Lozada, O. Olivares-Xometl, I.V. Lijanova, J. Arriola-Morales, J.C. Mendoza-Hérnandez, and G. Corro, *Int. J. Electrochem. Sci*., 14 (2019) 2655.
20. A. S. Fouda, M.M. Hegazi, and A. El-Azaly, *Int. J. Electrochem. Sci*., 14 (2019) 4668.
21. R. Hsissou, F. Benhiba, O. Dagdag, M. El Bouchti, K. Nouneh, M. Assouag, S. Briche, A. Zarrouk, and A. Elharfi, *J. Colloid Interf. Sci.*, 574 (2020) 43.
22. F. El-Hajjaji, M. Messali, M.V. Martinez de Yuso, E. Rodriguez-Castellon, S. Almutairi, T.J. Bandosz, and M. Algarra, *J. Colloid Interf. Sci*., 541 (2019) 418.

23. G. Vengatesh, and M. Sundaravadivelu, *J. Mol. Liq*., 287 (2019) 110906.
24. B. Tan, S. Zhang, W. Li, X. Zuo, Y. Qiang, L. Xu, J. Hao, and S. Chen, *J. Ind. Eng. Chem*., 77 (2019) 449.
25. M.B. Radovanović, and M.M. Antonijević, *J. Adhesion Sci. Technol*., 31 (2016) 369.
26. M.M. Antonijević,and S.M. Milić, *Mater. Chem. Phys*., 118 (2009) 385.
27. Y.J. Yang, Y. Li, L. Wang, H. Liu, D.M. Lu, L. Peng, *Int. J. Electrochem. Sci*., 14 (2019) 3375.
28. C. Wang, W. Gou, C. Liu, D. Fu, L. Zhou, C. Lai, B. Xie, and S. Zhu, *Int. J. Electrochem. Sci*., 14 (2019) 3443.
29. J. Tang, Y. Hu, H. Wang, Y. Zhu, Y. Wang, Z. Nie, Y. Wang, and B. Normand, *Int. J. Electrochem. Sci*.,14 (2019) 2246.
30. A. Singh, K.R. Ansari, D.S. Chauhan, M.A. Quraishi, H. Lgaz, and I.M. Chung, *J. Colloid Interf. Sci.*, 560 (2020) 225.
31. M.M. Solomon, S.A. Umoren, M.A. Quraishi, and M. Salman, *J. Colloid Interf. Sci.*, 551 (2019) 47.
32. M. Talari, S. Mozafari Nezhad, S.J. Alavi, M. Mohtashamipour, A. Davoodi, and S. Hosseinpour, *J. Mol. Liq.*, 286 (2019) 110915.
33. S. Tao, and H. Huang, *Int. J. Electrochem. Sci.*, 14 (2019) 5435.
34. L.O. Olasunkanmi, and E.E. Ebenso, *J. Colloid Interf. Sci.*, 561 (2020) 104.
35. B. Tan, S. Zhang, Y. Qiang, L. Guo, L. Feng, C. Liao, Y. Xu, and S. Chen, *J. Colloid Interf. Sci*., 526 (2018) 268.
36. Z.Z. Tasic, M.M. Antonijevic, M.B. Petrovic Mihajlovic, and M.B. Radovanovic, *J. Mol. Liq*., 219 (2016) 463.
37. I. Martinović, G.Z. Zora Pilić, L. Šušić, O. Kowalska, D. Petrović, F. Falak, and J. Mišković, *Int. J. Electrochem. Sci.*, 14 (2019) 4206.
38. Q.H. Zhang, B.S. Hou, and G.A. Zhang, *J. Colloid Interf. Sci.*, 572 (2020) 91.
39. P. Singh, D.S. Chauhan, S.S. Chauhan, G. Singh, and M.A. Quraishi, *J. Mol. Liq*., 286 (2019) 110903.
40. B. Tan, S. Zhang, Y. Qiang, L. Feng, C. Liao, Y. Xu, and S. Chen, *J. Mol. Liq*., 248 (2017) 902.
41. M.B. Petrović Mihajlović, M.B. Radovanović, Ž.Z. Tasić, and M.M. Antonijević, *J. Mol. Liq.*, 225 (2017) 127.
42. S. Y. Al-Nami, *Int. J. Electrochem. Sci.,* 14 (2019) 3986
43. B. Tan, S. Zhang, J. He, W. Li, Y. Qiang, Q. Wang, C. Xu, and S. Chen, *J. Mol. Liq.* 321 (2021) 114464.